ISIJ International, Vol. 46 (2006), No. 7, pp. 1020–1026

Properties of Dust Particles Sampled from Windboxes of an Iron Ore Sintering Plant: Surface Structures of Unburned Carbon

Naoto TSUBOUCHI, Shunsuke KUZUHARA, Eiki KASAI, Hiroyuki HASHIMOTO and Yasuo OHTSUKA

Research Center for Sustainable Materials Engineering, Institute of Multidisciplinary Research for Advanced Materials, Tohoku University, Katahira, Aoba-ku, Sendai 980-8577 Japan. E-mail: tsubon@tagen.tohoku.ac.jp

(*Received on February 7, 2006; accepted on March 31, 2006*)

Aiming to understand the formation mechanism of dioxins in the iron ore sintering process, dust samples obtained from some windboxes of a commercial iron ore sintering plant have been characterized with a powder X-ray diffraction (XRD), by the transmission electron microscope (TEM) equipped with an electron energy loss spectroscopy (EELS), and by the temperature-programmed desorption (TPD) and temperature-programmed oxidation (TPO) techniques. The elemental and XRD analyses reveal that the content of the Cl present in the samples ranges from 0.075 mass%-dry to 5.1 mass%-dry and tends to be higher at smaller dust particles, and that some of the Cl exists as KCl with the average crystalline size between 40 nm and 50 nm. Dust samples also contain a significant amount of unburned carbon, and the smallest dust particles, $<500\ \mu$m, show the highest C contents in many cases and consist partly of C, K, and Cl elements. The TPD and TPO experiments exhibit that the dust samples have several types of oxygen functional forms on the carbon surface, and the proportion of carboxyl and lactone/acid anhydride groups, which can be partly decomposed into CO_2 and carbon active sites at 150 to 500°C, tends to be larger at smaller dust particles. On the basis of the above results, the formation mechanism of chlorinated organic compounds including dioxins is discussed in term of interactions among HCl (and/or Cl_2), metallic chlorides, and carbon active sites.

KEY WORDS: iron ore sintering; windbox; dust; metallic chlorides; unburned carbon; surface oxygen complexes.

1. Introduction

Most of dioxins and chlorinated organic compounds emitted from commercial iron ore sintering processes are recognized to be formed *via de novo* synthesis involving unburned carbon (soot), that is, combustion residue of cokes as raw materials and carbonaceous particles derived from hydrocarbon components.[1–6] Various model experiments and equilibrium calculations have thus been carried out to make clear the factors controlling the synthesis and to elucidate possible mechanisms of dioxins formation. The principal results are summarized as follows:

(1) The formation of organic chlorides including dioxins is remarkable at around 300°C to 350°C.[4,5,7,8]
(2) The catalytic activity of metallic chlorides for the synthesis increases in the sequence of ($SnCl_2$, $CdCl_2$, $NiCl_2$, $FeCl_2$, $MnCl_2$, $CaCl_2$)<($PbCl_2$, $ZnCl_2$, $FeCl_3$)<$CuCl \ll CuCl_2$.[9–11]
(3) Alkali chlorides, such as NaCl and KCl, are also active for the high temperature synthesis, and their effectiveness are almost similar to that of $CaCl_2$.[10,12,13]
(4) As the rate of O_2-gasification at 300°C of carbonaceous materials increases, yields of organic chlorides increase remarkably.[10,11]

These observations strongly suggest that some metallic chlorides work efficiently as the catalysts for the dioxins synthesis, and that unburned carbon is the dominant carbon-source of organic chlorides including dioxins. It is therefore important to elucidate the chemical forms of metallic chlorides and the functionalities of unburned carbon emitted from commercial sintering processes. However, such approaches have not been made so far.[14]

In the sintering bed of iron ores, it is very difficult to identify or obtain a soot sample apart from other carbon-bearing materials because of its low concentration. On the other hand, the discharged gas from the sintering process contains significant amounts of dust particles including the fragments of the raw materials such as iron ores, limestone, and cokes. Unburned carbon and metallic chlorides are also contained in the dust particles. The present work thus aims first at examining the composition of dust samples collected from several windboxes of a commercial iron ore sintering plant, then at elucidating the functional forms of the unburned carbon present in the samples, and at approaching possible mechanisms for dioxins formation *via de novo* synthesis.

2. Experimental

2.1. Dust Samples

Dust samples were collected from several windboxes

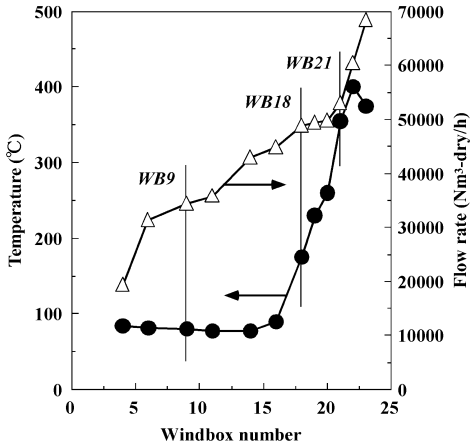

Fig. 1. Temperature and flow rate of outlet gas from windboxes.

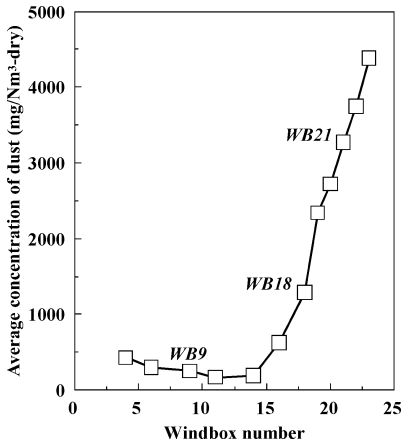

Fig. 2. Average concentration of dust present in windbox gas.

(denoted as WB) of a commercial iron ore sintering plant. The plant has a Dwight-Lloyd type machine with twenty-three WB, in which air is sucked downward through the sintering bed. **Fig. 1** shows the temperature and flow rate of discharged gas from each WB, and **Fig. 2** illustrates the average concentration of the dust present in the gas. These values tended to be higher at a larger WB number, that is, at the latter stage of the sintering process.

The sampling of the dust was carried out in the following manner. The gases were sucked by the constant velocity method from the ninth, eighteenth, and twenty-first WB and were passed over a membrane filter at a rate of 1×10^{-2} Nm^3-dry/min. The sampling was stopped before the filter was clogged with the dust particles by checking its pressure drop. Then, the filter was changed and the sampling was restarted. The continuous sampling time was between 15 min and 45 min, depending on the dust concentration. Fine solid materials remaining on the filter were collected carefully as dust samples, which are expressed according to the corresponding WB number as WB9, WB18, and WB21 throughout the present paper. All of them were sieved to the particles with size fraction of $<$500, 500–1000, or $>$1000 μm and subjected to the following characterization. The suffix "F (fine)", "M (medium)", or "C (coarse)" is added to the code name to denote these particle size ranges.

2.2. Dust Characterization

The contents of ten metals (Na, Mg, Al, Si, K, Ca, Fe, Cu, Zn, Pb) and water-soluble Cl present in all dust samples used were analyzed according to the corresponding Japanese Industrial Standard (JIS) methods. The Cl insoluble in water was determined by an ion chromatography using an aqueous solution of Cl-containing gas obtained by burning the residues after leaching of the water-soluble Cl up to 1 350°C. In this paper, the Cl content in dust samples is expressed as the sum of the water-soluble and insoluble Cl.

The powder X-ray diffraction (XRD) measurements of dust samples were made with Ni-filtered Cu-Kα radiation (30 kV, 40 mA) to identify crystalline phases present in the samples. The average crystalline size of KCl identified was determined by the Debye–Scherrer method.

Some dust samples were also characterized with a transmission electron microscope (TEM) equipped with an electron energy loss spectroscopy (EELS) at an accelerating voltage of 200 kV.

2.3. TPD and TPO Measurements

To evaluate quantitatively the functional forms of the unburned carbon present in the dust, the sample used was first subjected to the temperature-programmed desorption (TPD) experiment, in which about 100 mg of the dust charged into a cylindrical quartz reactor was heated at 10°C/min up to 950°C in a stream of high purity He ($>$99.99995%) and quenched to room temperature. In a temperature-programmed oxidation (TPO) run, the dust in the reactor after the TPD was reheated at 10°C/min up to 950°C under flowing 10 vol% O_2/He. The details of the apparatus have been reported elsewhere.[15)]

The amounts of CO_2 and CO evolved in the TPD and TPO runs were determined online at intervals of 2.5 min with a high-speed micro gas chromatograph, in which PP-Q or MS-5A column was used for the analysis of CO_2 or CO, respectively. Although CH_4 and C_2 hydrocarbons were also analyzed, no appreciable amounts of them were detectable in all cases.

3. Results and Discussion

3.1. Element Composition of Dust and Crystalline Forms

The composition of all of the dust samples used is provided in **Table 1**, where the content of each component is expressed in mass% on a dry sample basis. Fe was the main element for all samples, and the content was in the range of 46–60 mass%, followed by Ca in every case. On the other hand, Cu provided the lowest concentration, as small as $<$0.025 mass%, among eleven elements examined. As seen in Table 1, the contents of K and Cl tended to be higher at smaller dust particles, and the K and Cl in fine dust samples were 4.6 and 3.9 mass% for WB9, 5.2 and 5.1 mass% for WB18, and 0.92 and 1.7 mass% for WB21, respectively. These observations suggest that the K and Cl inherently present in iron ores and cokes as raw materials tend to be condensed predominantly in fine dust particles emitted from the sintering process.

Figure 3 shows the XRD profiles of dust samples recov-

Table 1. Analyses of dust samples used.

Sample[a]	Content (mass%-dry)										
	Na	Mg	Al	Si	K	Ca	Fe	Cu	Zn	Pb	Cl
WB9-F	0.39	0.34	0.71	1.4	4.6	5.5	46.0	0.010	0.067	0.39	3.9
WB9-M	0.066	0.59	0.88	1.8	0.39	5.7	55.2	0.004	0.033	0.021	0.30
WB9-C	0.033	0.69	0.95	2.1	0.13	5.0	57.7	0.003	0.021	0.001	0.075
WB18-F	0.44	0.33	0.74	1.4	5.2	3.6	48.8	0.023	0.067	0.53	5.1
WB18-M	0.056	0.47	0.81	1.5	0.28	4.2	56.9	0.004	0.027	0.015	0.39
WB18-C	0.036	0.73	0.86	2.0	0.14	4.4	56.8	0.004	0.023	0.001	0.66
WB21-F	0.11	0.36	0.81	1.5	0.92	4.6	55.8	0.006	0.032	0.073	1.7
WB21-M	0.051	0.49	0.80	1.6	0.30	3.9	57.8	0.003	0.025	0.023	0.67
WB21-C	0.029	0.41	0.69	1.6	0.14	3.4	59.8	0.003	0.034	0.001	0.086

[a]F, fine; M, medium; C, coarse.

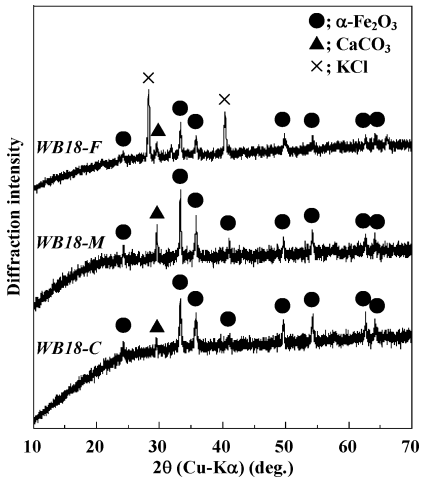

Fig. 3. XRD patterns of WB18 samples with different particle sizes.

Table 2. Species identified by XRD and average crystalline size of KCl.

Sample	XRD species identified[a]	KCl size[b] (nm)
WB9-F	KCl (s), α-Fe_2O_3 (m), $CaCO_3$ (w)	48
WB9-M	$K_2CO_3 0.5H_2O$ (vs), α-Fe_2O_3 (s), $CaCO_3$ (s)	–
WB9-C	α-Fe_2O_3 (m), $CaCO_3$ (vw)	–
WB18-F	KCl (s), α-Fe_2O_3 (m), $CaCO_3$ (w)	39
WB18-M	α-Fe_2O_3 (s), $CaCO_3$ (m)	–
WB18-C	α-Fe_2O_3 (s), $CaCO_3$ (vw)	–
WB21-F	KCl (vw), α-Fe_2O_3 (s), $CaCO_3$ (m)	40
WB21-M	α-Fe_2O_3 (s), $CaCO_3$ (w)	–
WB21-C	α-Fe_2O_3 (s), $CaCO_3$ (vw)	–

[a]Intensities designated as vw, very weak; w, weak; m, medium; s, strong; vs, very strong.
[b]Average crystalline size determined by the Debye-Scherrer method.

ered from WB18, and **Table 2** summarizes the XRD results of all samples used. Hematite (α-Fe_2O_3) was the predominant crystalline phase, irrespective of the type of the dust. The diffraction peaks of limestone ($CaCO_3$) were also observed in every case. The XRD signals attributable to KCl were detectable in all fine dust samples, and the average crystalline size was estimated to be 39–48 nm. There may be some possibility about the KCl sources. Inherent KCl in iron ores and cokes as raw materials, if present, may be considered as one possibility, because standard Gibbs free energy changes (ΔG) for the reaction of KCl with H_2O from the raw materials are +211 kJ/mol at 1 000°C and +189 kJ/mol at 1 500°C, which mean that KCl is very stable even in the coexistence of H_2O at high temperatures of ≥1 000°C. The KCl identified may thus come from the KCl inherently present in these raw materials. Another possibility may be secondary reactions of the dust with gaseous Cl-containing compounds. Since it has been reported that the Cl inherently present in iron ores and cokes is emitted mainly as HCl (usually 50–100 ppm in volume) upon combustion,[1,16] part of the HCl may react with O_2 in the sintering process to form Cl_2 according to the following equation, that is, the Deacon reaction.

$$2HCl + 1/2\,O_2 \rightarrow Cl_2 + H_2O \quad \text{.....(1)}$$

Thermodynamic calculations show that ΔG values for Eq. (1) are −36 kJ/mol at 50°C and −6 kJ/mol at 500°C, indicating significant driving forces for Cl_2 formation in the temperature region (Fig. 1) of the present WB. According to X-ray absorption near edge structure spectra of cokes, on the other hand, it has been reported that K present in cokes derived from bituminous coals exists mainly as amorphous or glassy K-containing aluminosilicates, for example, leucite ($KAlSi_2O_6$).[17,18] It might thus be reasonable to see that the KCl identified by XRD is formed through secondary reactions of HCl and/or Cl_2 with K_2CO_3 (Table 2) and $KAlSi_2O_6$ (Eqs. (2)–(5)).

$$K_2CO_3 + 2HCl \rightarrow 2KCl + CO_2 + H_2O \quad \text{.....(2)}$$

$$2KAlSi_2O_6 + 2HCl \rightarrow 2KCl + Al_2O_3 + 4SiO_2 + H_2O \quad \text{....(3)}$$

$$K_2CO_3 + Cl_2 + CO \rightarrow 2KCl + 2CO_2 \quad \text{.....(4)}$$

$$2KAlSi_2O_6 + Cl_2 + CO \rightarrow 2KCl + Al_2O_3 + 4SiO_2 + CO_2 \quad \text{.....(5)}$$

These reactions are favorable thermodynamically under the temperature conditions (Fig. 1) of the present WB, because ΔG values for Eqs. (2)–(5) at 50–500°C are in the range of −17 – −204 kJ/mol.

The TEM photograph of the WB18-F sample is shown in **Fig. 4**, and the result by the EELS analysis is provided in **Fig. 5**. As expected from the results in Tables 1, 2, and

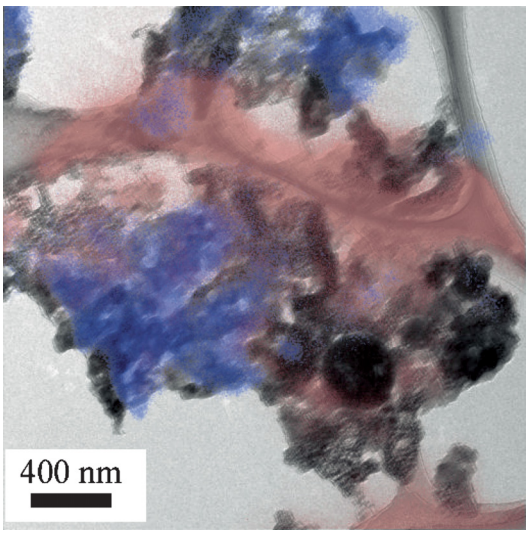

Fig. 4. TEM image of WB18-F dust: red, carbon; blue, chlorine; black, potassium.

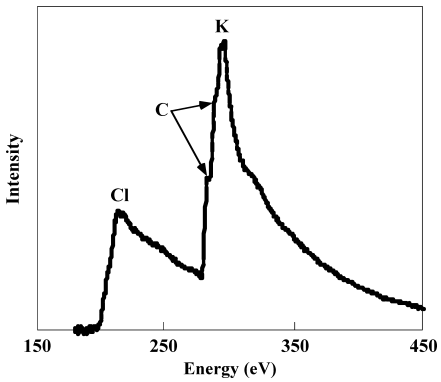

Fig. 5. EELS spectrum for point analysis of Fig. 4.

Fig. 3, part of the dust consisted of K and Cl elements. Interestingly, C element was also observed in the dust, though the EELS peaks were slightly broader (Fig. 5). Since it has been well-accepted that unburned carbon is the major carbon-source for *de novo* synthesis of dioxins and organic chlorides,[1–6] it is of interest to evaluate quantitatively the functional forms of the unburned carbon present in the dust samples used, which were thus subjected to the TPD/TPO runs. The results will be described in detail below.

3.2. TPD and TPO Behavior of Unburned Carbon

The examples for the rates of CO_2 and CO evolved in the TPD/TPO experiments of fine dust samples are given in **Fig. 6**, where each rate is expressed as micromoles of CO_2 or CO per minute and gram of feed dust. In the TPD runs, CO_2 formation started at a low temperature of 200°C in every case, and the WB9-F, WB18-F, and WB21-F provided the broad spectra with the peak temperature of 660°C, 640°C, and 580°C, respectively. On the other hand, CO started to evolve at 450–500°C with the two samples except the WB21-F, for which CO was very small, and the rates were smaller than those of CO_2 in all cases. Similar results were also observed for the dust samples with medium and coarse particle sizes. As seen in Fig. 6, both CO_2 and CO formed during TPO runs showed the rate profiles peaking at 680–700°C, irrespective of the kind of the dust, and the

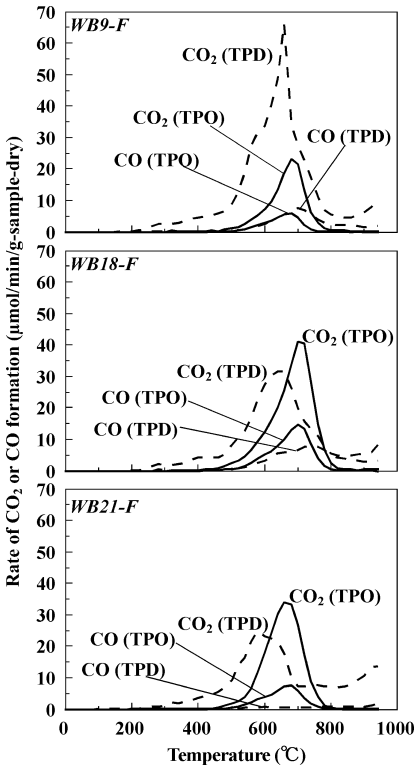

Fig. 6. Rates of CO_2 and CO formation in the TPD/TPO runs of fine dust samples.

rates of CO_2 formation were always higher than those of CO formation.

The TPD/TPO results for all of the dust samples used are summarized in **Table 3**, where the content of the carbon present in each dust is calculated from the total amounts of CO_2 and CO formed in both processes. The carbon content in the WB21-F, WB21-M, or WB21-C was estimated to be 3.3 mass%-dry, 3.1 mass%-dry, or 1.8 mass%-dry, respectively. These values were nearly equal to carbon contents determined with a conventional, combustion-type elemental analyzer, as shown as the figures in parentheses in Table 3. Such a good agreement indicates that the combination of the present TPD and TPO methods can detect almost all of the carbon present in the dust. The carbon contents in all dust samples examined were in the range of 1.7–4.6 mass%-dry, and the WB9-C and WB18-C had the lowest and highest content, respectively.

As seen in Table 3, yields of CO_2 evolved in the TPD runs were about 4–20 times those of CO, and yield of CO_2 or CO among all dust samples increased in the following order in many cases:

CO_2: M dust (30–35 C-%)<C dust (25–45 C-%)<F dust (46–68 C-%)

CO: M dust (2–3 C-%)≒C dust (2–4 C-%)<F dust (5–13 C-%)

Yields of CO_2 formed during the TPO were always higher than those of CO, and both tended to increase in the following sequence:

CO_2: F dust (17–32 C-%)<M dust (49–55 C-%)<C dust (47–65 C-%)

Table 3. Carbon contents in dust samples used and yields of CO_2 and CO evolved during TPD and TPO runs.

Sample	Carbon content[a]	TPD in high purity He		TPO in 10 vol% O_2/He	
		CO_2	CO	CO_2	CO
	(mass%-dry)	(C-%)[b]	(C-%)[b]	(C-%)[b]	(C-%)[b]
WB9-F	3.9	68.1	10.7	16.9	4.3
WB9-M	3.3	35.4	2.8	48.8	13.0
WB9-C	1.7	44.5	4.4	47.2	3.9
WB18-F	4.3	45.9	12.8	30.8	10.5
WB18-M	3.8	30.4	2.3	53.6	13.7
WB18-C	4.6	24.8	2.4	65.4	7.4
WB21-F	3.3 (3.0)[c]	55.8	4.5	32.4	7.3
WB21-M	3.1 (3.1)[c]	30.6	1.6	54.6	13.2
WB21-C	1.8 (1.8)[c]	33.7	2.3	57.4	6.6

[a]Estimated by CO_2 and CO evolved during TPD and TPO runs.
[b]Based on carbon content.
[c]Carbon content determined with a conventional, combustion-type elemental analyzer.

CO: C dust (4–7 C-%)<F dust (4–11 C-%)
<M dust (13–14 C-%)

It is evident in Fig. 6 and Table 3 that the TPD/TPO behavior of unburned carbon depends strongly on the type of the dust. It is reasonable to suppose that such differences can affect *de novo* synthesis of organic chlorides including dioxins, because the unburned carbon is the dominant carbon-source of chlorinated aromatic species.[1–6)]

3.3. Structures of Unburned Carbon

The different rates and yields of CO_2 and CO observed in the TPD/TPO experiments of several dust samples may originate from the differences in surface oxygen complexes on the carbon present in these samples. According to earlier studies on surface functionalities of coal chars and carbons using the TPD technique,[19–23)] CO_2 evolved arises mainly from decomposition reactions of carboxyl groups, lactone/acid anhydride groups, and inherently-present $CaCO_3$. In order to examine the sources of CO_2 evolved in the present TPD process, the profiles for the CO_2 formation observed were curve-fitted with the least-squares method using Gaussian peak shapes. In this method, the CO_2 peak temperature and full width at half maximum of each compound were assumed at 350±10°C and 200±10°C for carboxyl groups,[20)] 620±10°C and 200±10°C for lactone/acid anhydride groups,[22)] and 650±10°C and 60±10°C for $CaCO_3$,[24)] respectively. The typical deconvolution profiles for the WB9-F, WB9-M, and WB9-C are illustrated in **Fig. 7**. Very good curve resolution was obtained, and the reproducibility fell within ±3% in every case when the curve-fitting analysis was repeated at least twice. As seen in Fig. 7, 85–90% of the CO_2 evolved from the WB9 arose from decomposition reactions of both lactone/acid anhydride groups and $CaCO_3$, almost independently of the size of the dust. The sources of the CO_2 observed above 820°C are not clear at present, but the CO_2 evolution might be caused by the catalysis of some minerals present in the dust samples. This point should be clarified in the future work.

With regard to CO released during TPD, it has been widely accepted that the CO originates mostly from ketone, ether, and phenolic groups.[21,23)] Further, CO_2 and CO

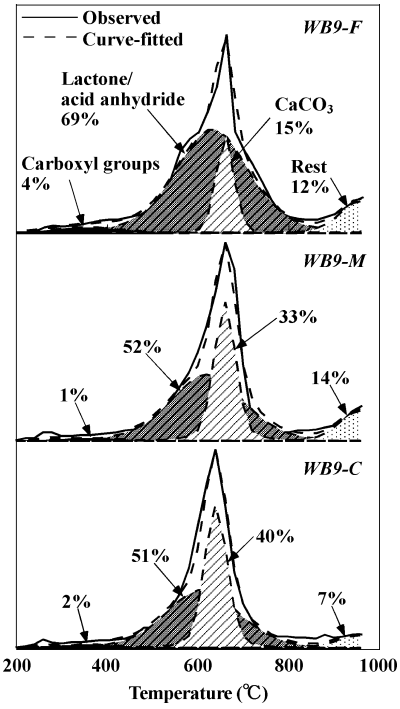

Fig. 7. Deconvolution of the rate profiles for CO_2 formation observed in the TPD process of WB9 samples.

formed during TPO arise probably from carbon atoms in condensed aromatic structures remaining after the complete release of surface oxygen complexes on carbonaceous materials.[25)] On the basis of this information and the curve-fitting data (Fig. 7), the sources of CO_2 and CO evolved in the TPD/TPO runs of all dust samples used are estimated and summarized in **Fig. 8**, where the proportion of each component is expressed in percent of total carbon (Table 3) in each dust sample. The proportion of carboxyl, lactone/acid anhydride, and ketone/ether/phenolic groups was the largest at the smallest dust particles, regardless of the number of the WB, whereas $CaCO_3$ and carbon atoms in thermally stable aromatic ring structures, denoted as other forms, tended to be higher at larger dust particles. It is well-known that surface oxygen complexes on carbonaceous materials are decomposed into CO_2 and CO during gasification to form

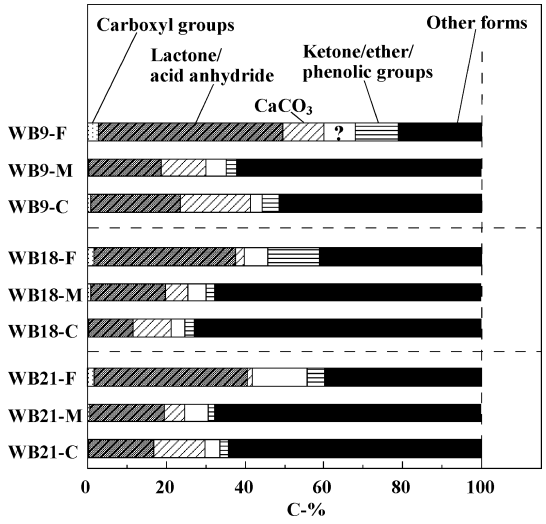

Fig. 8. Functional forms of unburned carbon estimated by the TPD/TPO methods.

carbon active sites (that is, edge carbon).[26] When the complexes and active sites are designated as C(OO) (and/or C(O)) and C( ), respectively, decomposition reactions of the former species can be expressed as follows:

$$C(OO) \rightarrow C(\ ) + CO_2 \quad \text{.....(6)}$$

$$C(O) \rightarrow C(\ ) + CO \quad \text{.....(7)}$$

It has been reported that the reactivity of carbon active sites is about 100–1 000 times that of carbon atoms in condensed aromatic structures, that is, basal plane carbon.[26] It may thus be reasonable to see that the C( ) derived from carboxyl and lactone/acid anhydride groups, which are decomposed under the present WB's temperature conditions (Figs. 1 and 7) that are almost the same as the temperature region for *de novo* synthesis, is the active carbon site for the formation of dioxins and organic chlorine compounds.

3.4. Possible Routes for *de Novo* Synthesis of Organic Chlorine Compounds Including Dioxins

As mentioned above, the dust samples contain KCl with the average crystalline size of 40–50 nm (Table 2), significant amounts of unburned carbon (Table 3), and very low contents of Cu element (Table 1). Further, the smallest dust particles with $<500\ \mu$m are composed partly of C, K, and Cl elements (Figs. 4 and 5). In addition, the unburned carbon has a slight amount of carboxyl groups and a relatively large amount of lactone/acid anhydride groups (Fig. 8), and part of these O-containing species is decomposed into CO_2 and carbon active sites (Fig. 7) in the temperature region (150–500°C) where *de novo* synthesis proceeds. It has been recently suggested that such oxygen functional groups on unburned carbon surface play crucial roles in the formation of chlorinated aromatic structures.[14,27,28] It has been also reported that the K-catalyzed gasification of coal chars and carbons proceeds through the mechanism involving phenoxide ($C–O^-–K^+$) formed by the reaction of K_2CO_3 and carbon substrate.[29] It is thus speculated as one possibility that *de novo* synthesis in the presence of K_2CO_3 occurs *via* the following mechanism. HCl (and/or Cl_2) once-evolved in the sintering process might react with $C–O^-–K^+$ produced by the interaction between K_2CO_3 (Table 2) and carbon active sites (C( )) to provide Cl-containing intermediates, for example, $C–O^-–K^+–Cl^-–H^+$, which may subsequently undergo decomposition reactions into chemisorbed HCl species (C(HCl)), covalent C–Cl bonds (C(Cl), and/or KCl. The presence of these species was speculated by the X-ray photoelectron spectroscopy spectra of activated carbon (K, 0.5 mass%-dry) treated with HCl at 500°C.[30] The C(HCl) and C(Cl) species, if present actually, may be transformed to dioxins and organic chlorides by the catalytic effect of some minerals.

It has been reported that metallic chlorides present in unburned carbon work efficiently as not only the Cl-sources but also the catalysts (or promoter materials) for *de novo* synthesis.[9–13] The catalysis of dioxins formation by metallic chlorides is thus considered as another possibility. According to earlier work, the Cu element (Table 1) determined by the elemental analysis is probably present as the chloride and oxide forms.[31] It is therefore possible that fine-particles of KCl and copper chlorides might react with C( ) to form $C–O^-–K^+–Cl^-–H^+$ and $C–O^-–Cu^+–Cl^-–H^+$ intermediates, which may subsequently decompose into provide organic chlorine compounds including dioxins. However, the contribution of this route to dioxins formation is still uncertain, because KCl and CuCl are rather stable thermodynamically at 150–500°C where *de novo* synthesis proceeds considerably.

Since both the contents of the C, K, Cu, and Cl present in the dust samples examined (Tables 1 and 3) and the proportion of surface oxygen complexes on the unburned carbon (Fig. 8) tend to be lager at smaller dust particles, dioxins formation may proceed significantly at fine dust particles than at the coarse ones. To clarify *de novo* synthesis mechanisms in detail should be the subject of future study.

4. Conclusions

Dust samples collected from windboxes of a commercial iron ore sintering plant were characterized by means of XRD, TEM-EELS and TPD/TPO methods, and the following conclusions are summarized:

(1) Chlorine element exists in all the dust samples in the range between 0.075 mass%-dry and 5.1 mass%-dry, and the smallest dust particles, $<500\ \mu$m, show the highest Cl contents, regardless of the number of the windbox. The XRD reveals the presence of KCl with the average crystalline size of 40–50 nm.

(2) Dust samples contain unburned carbon, and the concentration range is from 2 mass%-dry to 5 mass%-dry. The carbon content tends to be larger at smaller dust particles. The TEM-EELS analysis shows that part of the smallest dust particles are comprised of C, K, and Cl elements.

(3) The results of the TPD indicate the formation of carboxyl and lactone/acid anhydride groups on the surface of the unburned carbon, and the proportion of these oxygen complexes tends to increase with decreasing particle size of the dust.

(4) On the basis of the above results, it can be speculated that carbon active sites derived from the surface oxygen complexes may work efficiently as *de novo* synthesis sites of dioxins and organic chlorine compounds.

Acknowledgment

One of the authors (NT) gratefully acknowledges the Steel Industry Foundation for the Advancement of Environmental Protection Technology.

REFERENCES

1) E. Kasai, T. Aono, Y. Tomita, M. Takasaki, N. Shiraishi and S. Kitano: *ISIJ Int.*, **41** (2001), 86.
2) E. Kasai, Y. Hosotani, T. Kawaguchi, K. Nushiro and T. Aono: *ISIJ Int.*, **41** (2001), 93.
3) E. Kasai, T. Kawaguchi, T. Aono, Y. Hosotani, Y. Tomita and H. Noda: Proc. of 6th Int. Conf. on Technologies and Combustion for a Clean Environment, Vol. 1, OPET Portugal, Porto, Portugal, (2001), 245.
4) A. Buekens, L. Stieglitz, K. Hell, H. Huang and P. Segers: *Chemosphere*, **42** (2001), 729.
5) K. Suzuki, E. Kasai, T. Aono, H. Yamazaki and K. Kawamoto: *Chemosphere*, **54** (2004), 97.
6) M. Nakano, Y. Hosotani and E. Kasai: *ISIJ Int.*, **45** (2005), 609.
7) P. F. Tan and D. Neuschutz: *Metall. Mater. Trans. B-Proc. Metall. Mater. Proc. Sci.*, **35** (2004), 983.
8) S. Kasama, Y. Yamamura and K. Watanabe: *Tetsu-to-Hagané*, **91** (2005), 745.
9) L. Stieglitz, H. Vogg, G. Zwick, J. Beck and H. Bautz: *Chemosphere*, **23** (1991), 1255.
10) S. Kuzuhara, H. Sato, E. Kasai and T. Nakamura: *Environ. Sci. Technol.*, **37** (2003), 2431.
11) S. Kuzuhara, H. Sato, E. Kasai and T. Nakamura: *Organohalogen Compounds*, **63** (2003), 151.
12) R. Addink and E. R. Altwicker: *Environ. Eng. Sci.*, **15** (1998), 19.
13) S. Kuzuhara, E. Kasai, T. Nakamura and E. Shibata: *Organohalogen Compounds*, **50** (2001), 422.
14) N. Tsubouchi, E. Kasai, K. Kawamoto, H. Noda, Y. Nakazato and Y. Ohtsuka: *Tetsu-to-Hagané*, **91** (2005), 751.
15) Y. Ohtsuka, C. Xu, D. Kong and N. Tsubouchi: *Fuel*, **83** (2004), 685.
16) E. Kasai and T. Aono: *Tetsu-to-Hagané*, **87** (2001), 228.
17) C. L. Spiro, J. Wong, F. W. Lytle, R. B. Greegor, D. H. Maylotte and S. H. Lamson: *Fuel*, **65** (1986), 327.
18) G. P. Huffman, F. E. Huggins, R. W. Shoenberger, J. S. Walker, F. W. Lytle and R. B. Greegor: *Fuel*, **65** (1986), 621.
19) Y. Otake and R. G. Jenkins: *Carbon*, **31** (1993), 109.
20) Q-L. Zhuang, T. Kyotani and A. Tomita: *Carbon*, **32** (1994), 539.
21) U. Zielke, K. J. Huttinger and W. P. Hoffman: *Carbon*, **34** (1996), 983.
22) Q-L. Zhuang, T. Kyotani and A. Tomita: *Energy Fuels*, **8** (1994), 714.
23) B. Marchon, J. Carrazza, H. Heinemann and G. A. Somorjai: *Carbon*, **26** (1988), 507.
24) Y. Ohtsuka and A. Tomita: *Fuel*, **65** (1986), 1653.
25) H. Aso, K. Matsuoka, A. Sharma and A. Tomita: *Energy Fuels*, **18** (2004), 1309.
26) L. R. Radovic, A. A. Lizzio and H. Jiang: Fundamental Issues in Control of Carbon Gasification Reactivity, ed by J. Lahaye and P. Ehrburger, Kluwer Academic Publishers, Dordrecht, The Netherlands, (1991), 235.
27) N. Tsubouchi, S. Ohtsuka, Y. Nakazato and Y. Ohtsuka: *Energy Fuels*, **19** (2005), 554.
28) M. Takeda, A. Ueda, H. Hashimoto, T. Yamada, N. Suzuki, M. Sato, N. Tsubouchi, Y. Nakazato and Y. Ohtsuka: *Fuel*, **85** (2006), 235.
29) I. L. C. Freriks, H. M. H. van Xechem, J. C. M. Stuiver and R. Bouwman: *Fuel*, **60** (1981), 463.
30) N. Tsubouchi, Y. Nakazato, H. Kawashima and Y. Ohtsuka: Proc. of 2005 Int. Conf. on Coal Science and Technology, ICCS&T International Organizing Committee, Ibaraki, Japan, (2005), CD-ROM (paper no. 2P105).
31) M. Takaoka, A. Shiono, K. Nishimura, T. Yamamoto, T. Uruga, N. Takeda, T. Tanaka, K. Oshita, T. Matsumoto and H. Harada: *Organohalogen Compounds*, **66** (2004), 1103.